ELSEVIER

Modeling and electrokinetic evidences on the processes of the Al(III) sorption continuum in $SiO_{2(s)}$ suspension

Wen Hui Kuan,[a,*] Shang Lien Lo,[b] and Ming Kuang Wang[c]

[a] *Department of Environmental and Safety Engineering, Ming-Chi Institute of Technology, 84, Gunjuan Rd., Taishan, Taipei Hsien 243, Taiwan*
[b] *Graduate Institute of Environmental Engineering, National Taiwan University, Taipei 106, Taiwan*
[c] *Department of Agriculture Chemistry, National Taiwan University, Taipei 106, Taiwan*

Abstract

Reactions of Al(III) at the interface between $SiO_{2(s)}$ and aqueous solution were characteristically and quantitatively studied using electrophoretic methods and applying a surface complexation/precipitation model (SCM/SPM). The surface and bulk properties of Al(III)/SiO$_2$ suspensions were determined as functions of pH and initial Al(III) concentration. Simulated modeling results indicate that the SCM, accounting for the adsorption mechanism, predicts sorption data for low surface coverage only reasonably well. Al(III) hydrolysis and surface hydroxide precipitation must be invoked as the Al(III) concentration and/or pH progressively increase. Accordingly, the three processes in the Al(III) sorption continuum, from adsorption through hydrolysis to surface precipitation, could be identified by the divergence between the SCM/SPM predictions and the experimental data. $SiO_{2(s)}$ suspensions with low Al(III) concentrations (1×10^{-4} and 1×10^{-5} M) exhibit electrophoretic behavior similar to that of a pure $SiO_{2(s)}$ system. In Al(III)/SiO$_2$ systems with high Al concentrations of 1×10^{-3}, 5×10^{-3} and 1×10^{-2} M, three charge reversals (CR) are observed, separately representing, in order of increasing pH, the point of zero charge (PZC) on the SiO_2 substrate (CR1), the onset of the surface precipitation of Al hydroxide (CR2), and at a high pH, the PZC of the Al(OH)$_3$ coating (CR3). Furthermore, in the 1×10^{-3} M Al(III)/SiO$_{2(s)}$ system, CR2 is consistent with the modeling results of SCM/SPM and provides evidence that Al(III) forms a surface precipitate on $SiO_{2(s)}$ at pH above 4. $SiO_{2(s)}$ dissolution was slightly inhibited when Al(III) was adsorbed onto the surface of $SiO_{2(s)}$, as compared to the dissolution that occurs in a pure $SiO_{2(s)}$ suspension system. Al hydroxide surface precipitation dramatically reduced the dissolution of $SiO_{2(s)}$ because the Al hydroxide passive film inhibited the corrosion of the $SiO_{2(s)}$ surface by OH$^-$ ions.
© 2004 Elsevier Inc. All rights reserved.

Keywords: Al(III); Interface reactions; SiO$_2$; Electrophoretic method; Surface complexation model; Surface precipitation model

1. Introduction

Silicon is the second most abundant element in the earth's crust and is present as silicates and silica. Iler [1] divided silica into five different phases, of which anhydrous and hydrous amorphous silica are the most important from a colloidal perspective, since it is this phase that forms colloidal and microporous structures. In acidic lakes and streams throughout the world, aluminum is present in concentrations from several µmol/l to several hundred µmol/l [2], that is, at a level toxic to aquatic life [3]. Since the toxicity of Al depends strongly on its speciation (free and complexed Al)

and mobility (soluble, colloid, or precipitated) [4,5], its interaction with silica may significantly alter the bioavailability of this element and its detrimental effects on aquatic organisms [6,7]. In the water-treatment industry the interactions between silica and aluminum also play a determining role, because Al salts are common coagulants and silica is a prevalent constituent of solid matter in raw water. Moreover, hydrolyzed aluminum is used to set rosin and dyes in the production of paper and to improve the retention of fillers. The increased use of hydrolyzed aluminum salts has heightened commercial and research interest in aluminum hydrolysis [8,9]. A number of studies on aluminum hydrolysis have emphasized the stoichiometry or kinetics of complex hydrolysis, precipitation, and surface chemical reactions of a pure aluminum system [9,10]. Some researchers [11–14]

have pointed out that soluble aluminum has a high potential to form mixed oxides with other component oxides in natural environments, and the characteristics of such mixed oxides deviate significantly from either average collective properties for the group or a collection of discrete pure solid phases. However, the understanding of when and how the sorption continuum for Al(III), from soluble free ions to a surface or bulk oxide precipitate, proceeds in SiO$_{2(s)}$ suspensions is quite limited. Limited knowledge of these processes has restricted the accurate prediction of the distribution of Al(III) in aquatic systems and the adsorption properties of other trace elements onto the undefined surfaces of these mixed oxides.

When a metal ion is present in an oxide suspension system, a sorption continuum [15] may occur from mononuclear adsorption to hydrolysis, to multinuclear adsorption, or to precipitation on the surface of oxide or in bulk solution; during these processes, system pH or sorbate/sorbent ratios increase [16–19]. At a low pH or sorbate/sorbent ratio, cations coordinate with surface functional groups of an oxide; the enhanced interaction between adjacent cations results in a sorption continuum with pH and/or the sorbate/sorbent ratio increasing. Because adsorption, hydrolysis, and precipitation of Al(III) occur over a very narrow pH range, each process of the sorption continuum is difficult to interpret and distinguish [20,21]. Xu et al. [22] also indicated that such processes can proceed simultaneously, and distinguishing them requires analytical methods with molecular-scale resolution.

The following definitions are adopted in the discussion of the mechanism of the interface reactions. According to the relative concentrations and contact methods, interactions between hydrous oxides and metals include (1) sorption, referring to the uptake of a dissolved metal by a solid phase, irrespective of the mechanism [16,23,24]; (2) adsorption, referring to a surface complexation reaction between surface sites and a metal sorbate [25]; and (3) surface precipitation, referring to the formation of a precipitate, induced by the sorbent surface under solution conditions that are undersaturated with respect to any known phase [26–28]. Depending on the type of interaction, metals exhibit various solubilities that can markedly alter their environmental mobility and removal efficiency during wastewater treatment [29–31].

This study aims to identify the reactions that occurred during this sorption continuum of Al(III) in SiO$_{2(s)}$ suspension and to clarify how environmental conditions influence these processes. The effects of a wide range of sorbate-to-sorbent ratios and pH were modeled using SCM/SPM to clarify the onset of each process in the sorption continuum. Electrokinetic measurements were performed to determine the nature of the Al(III) interaction with the SiO$_{2(s)}$ surface [32]. The measurement of silica dissolution yielded information on the onset of surface precipitation.

2. Materials and methods

2.1. Batch experiments

Batch experiments concerning Al(III) sorption onto SiO$_2$ were conducted in 50-ml polypropylene bottles with caps. The used silica (SiO$_2$) was Cab-O-Sil M5 (Cabot Corp., Tuscolca, IL), amorphous and fumed silica with a BET surface area of 200 m^2/g (analyzed by ASAP 2000). Before the batch experiments were performed, the SiO$_2$ suspension was aged at 25 °C in an N$_2$ atmosphere for 2 h.

Solutions were prepared using reagent-grade chemicals and Millipore-Q water, following standard methods [33]. The initial concentration of Al(III) (Al(NO$_3$)$_3$·9H$_2$O) was 0–1 × 10^{-2} M; the SiO$_2$ concentration was maintained at 1 g/l, and the background electrolyte concentration was adjusted to 0.1 M by KNO$_3$ electrolyte solution. All experiments were performed at 25 °C, after adjustment to the desired pH using KOH and HNO$_3$ solutions, with shaking at 200 rpm. Since preliminary kinetic experiments suggested that pseudo-equilibrium was reached within 24 h, 24 h was selected as the reaction time for the equilibrium experiments [34].

To elucidate these processes in the sorption continuum, samples were prepared in which SiO$_{2(s)}$ powder was equilibrated with Al(III) aqueous solutions with concentrations from undersaturated to oversaturated, with respect to the bulk phase precipitation in the absence of a solid sorbent. Two parameters, pH and total Al(III) concentration, were studied in batch experiments to determine sorption pH edges and isotherms, respectively. After the reaction, a subsample of the suspension was taken for electrophoresis measurements; the rest of the suspension was centrifuged (Kubota 6800) at 10,000 rpm for 15 min and the supernatant was passed through a 0.2-µm membrane filter to analyze the soluble Al and the Si dissolved out of bulk SiO$_{2(s)}$ solid by an ICP-AES (Perkin–Elmer, Optima 2000DV).

2.2. Electrophoresis measurements

Electrophoretic mobility (EM) was measured at various pH and Al(III) concentrations to detect changes in net total particle surface charge density associated with the sorption of Al(III). The electrophoretic mobility of the particles in SiO$_2$ suspensions with various amounts of Al(III) at pH values between 1.5 and 12.0 was measured using a laser Doppler electrophoretic light-scattering apparatus (Malvern Instrument, Zetasizer 2000). Triplicate measurements were made in crossed-beam mode with a 30-s count time, an applied voltage of 150 V, and a modulator frequency of 1000 Hz.

2.3. Modeling approaches

Three categories of surface reaction were considered—surface complexation, surface precipitation, and bulk precip-

Table 1
Category of surface reactions

Category	Applied model	Forming species	Abbreviation
Surface complexation	SCM	Adsorption of hexaqua-Al^{3+} ion ($Al(H_2O)_6^{3+}$) onto $SiO_{2(s)}$	AA
		Adsorption of 1st hydrolyzed hexaqua-Al^{3+} ion ($Al(OH)(H_2O)_5^{2+}$) onto $SiO_{2(s)}$	AH
Surface precipitation	SPM	Coprecipitation of Al(III) hydroxide phase as a solid solution with the original $SiO_{2(s)}$ surface phase	PS
Bulk precipitation		Precipitation of $Al(OH)_{3(s)}$ in bulk solution	PB

Table 2
Fixed parameters for modeling with SCM and SPM

Site concentration of $SiO_{2(s)}$ (mmol/g)	1.67[a]
Surface area of $SiO_{2(s)}$ (m^2/g)	200[b]
$\log K_{a1}^{int}$	−1.5[a]
$\log K_{a2}^{int}$	−5.5[a]
$\log K_{sp\_Al}$	10.38[c]
$\log K_{sp\_Si}$	−2.74[c]

[a] Meng and Letterman [13,14].
[b] Measured in this study.
[c] Database of MINTEQA2 program.

itation—to describe the sorption continuum. In each reaction category, Al(III) forms several surface species, depending on the system conditions (Table 1).

2.3.1. Surface complexation model (SCM)

The geochemical speciation code MINTEQA2, Version 3.11 [35], was used to simulate the equilibrium partition of Al(III) in the $SiO_{2(s)}$/aqueous solution. The $SiO_{2(s)}$ surface parameters were adopted from the work of Meng and Letterman [13,14] and are presented in Table 2. Both the diffuse layer model (DLM) and the database included in the MINTEQA2 were used for surface complexation modeling. The DLM was a type of simple two-layer model, including one planar surface layer and one diffuse layer of counterions [36]. The exponential coulombic term derived from Gouy and Chapman's electrical double layer theory (EDL) was introduced to correct the surface-reaction mass-law constants for surface charge effects [32]. Table 3 summarizes the surface reactions considered in the SCM (Eqs. (1)–(4)).

2.3.2. Surface precipitation model (SPM)

Farley et al. [37] extended the DLM to include surface precipitation by taking into account the formation of a new surface phase, which is described as an ideal solid solution [38,39] of $Me(OH)_{2(s)}$ and $Fe(OH)_{3(s)}$. This approach yields a continuum between the adsorption of a solute on a surface and the precipitation of this solute as a new bulk solid phase. In this study, the model was modified and applied to the Al(III)/$SiO_{2(s)}$ system.

The success of the surface precipitation model follows from the fact that it provides a mathematical approach to increasing the activity of the coprecipitating solid metal hydroxide phase continuously from near zero to unit activity as the amount of surface precipitate that forms increases. This continuous increase is accomplished by assuming that an ideal solid solution is generated by

$$\{Al(OH)_{3(s)}\} = \frac{[Al(OH)_{3(s)}]}{T_s} \tag{5}$$

and

$$\{SiO_{2(s)}\} = \frac{[SiO_{2(s)}]}{T_s}, \tag{6}$$

where { } and [ ], respectively, represent the activity and molal concentration of the corresponding species, and T_s represents the total mass of solid material in solid solution and is given by

$$T_s = [Al(OH)_{3(s)}] + [SiO_{2(s)}]. \tag{7}$$

Additionally, an ideal solid solution is assumed, so

$$\{Al(OH)_{3(s)}\} + \{SiO_{2(s)}\} = 1. \tag{8}$$

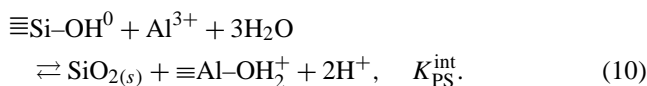This representation allows the solubility of the aluminum hydroxide phase to decline at lower surface coverages. For

Table 3
Surface reactions considered in SCM

Reaction	Equilibrium constant expression	
Surface ionization		
$SOH + H^+ \rightleftharpoons SOH_2^+$	$K_{a1}^{int} = \exp(F\varphi/RT)[SOH_2^+]/[SOH][H^+]$	(1)
$SOH \rightleftharpoons SO^- + H^+$	$K_{a2}^{int} = \exp(-F\varphi/RT)[SO^-][H^+]/[SOH]$	(2)
Surface complexation		
$SOH + Al^{3+} \rightleftharpoons SOAl^{2+} + H^+$	$K_{AA}^{int} = \exp(2F\varphi/RT)[SOAl^{2+}][H^+]/[SOH][Al^{3+}]$	(3)
$SOH + Al^{3+} + H_2O \rightleftharpoons SOAlOH^+ + 2H^+$	$K_{AH}^{int} = \exp(F\varphi/RT)[SOAlOH^+][H^+]^2/[SOH][Al^{3+}]$	(4)

F: Faraday constant; φ: the potential at the $SiO_{2(s)}$ surface; R: gas constant; T: absolute temperature.

example, the aluminum hydroxide phase forms when the Al(III) ion activity product (IAP) is exceeded, according to
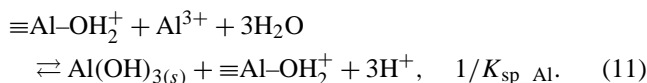
$$IAP = \{Al^{3+}\}\{OH^-\}^3 = \{Al(OH)_{3(s)}\}K_{sp\_Al}, \quad (9)$$

where K_{sp_Al} is the thermodynamic solubility product constant of $Al(OH)_{3(s)}$. According to Eq. (5), as $\{Al(OH)_{3(s)}\}$ decreases, the value of the IAP required for the onset of precipitation decreases. Hence, surface precipitation can occur at Al(III) ion concentrations and pH values below those required for precipitation of the pure solid phase from aqueous solution. A solid-phase activity continuously increasing from almost zero to unity has been found to be necessary to enable the solid solution model to describe Al(III) ion sorption as a function of the changing surface coverage.

In this model, Al(III) at the $SiO_{2(s)}$/aqueous solution interface is treated as a surface species, while Al(III) is not in direct contact with the solution phase; that is, it is buried under the $SiO_{2(s)}$/aqueous solution interface and is treated as a solid species (denoted by subscript (s)) that forms a solid solution. Surface precipitation reactions involved in the uptake of Al(III) by $SiO_{2(s)}$ can then be written as follows:

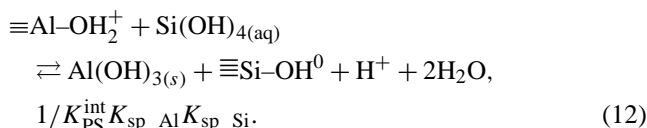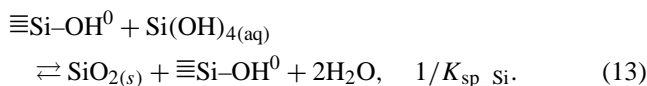Adsorption of Al(III) onto $SiO_{2(s)}$

$$\equiv\!Si\text{–}OH^0 + Al^{3+} + 3H_2O$$
$$\rightleftarrows SiO_{2(s)} + \equiv\!Al\text{–}OH_2^+ + 2H^+, \quad K_{PS}^{int}. \quad (10)$$

Precipitation of Al(III)

$$\equiv\!Al\text{–}OH_2^+ + Al^{3+} + 3H_2O$$
$$\rightleftarrows Al(OH)_{3(s)} + \equiv\!Al\text{–}OH_2^+ + 3H^+, \quad 1/K_{sp\_Al}. \quad (11)$$

Adsorption of $Si(OH)_4$ on $Al(OH)_{3(s)}$

$$\equiv\!Al\text{–}OH_2^+ + Si(OH)_{4(aq)}$$
$$\rightleftarrows Al(OH)_{3(s)} + \equiv\!Si\text{–}OH^0 + H^+ + 2H_2O,$$
$$1/K_{PS}^{int}K_{sp\_Al}K_{sp\_Si}. \quad (12)$$

Precipitation of $Si(OH)_4$

$$\equiv\!Si\text{–}OH^0 + Si(OH)_{4(aq)}$$
$$\rightleftarrows SiO_{2(s)} + \equiv\!Si\text{–}OH^0 + 2H_2O, \quad 1/K_{sp\_Si}. \quad (13)$$

The surface symbols $\equiv$ and $\equiv$ are used to denote the bonds of the cations with the surface of the solid, and have different meanings for Si(IV) and Al(III): $\equiv\!Si\text{–}OH^0$ represents $[SiO_2]_n$ because SiO_2 is a tetrahedron, with four O atoms bonded to each Si atom, and $\equiv\!Al\text{–}OH^0$ represents $[Al(OH)_3]_n$ because $Al(OH)_3$ is an octahedron, with three O atoms bonded to each Al atom. Thus reactions (10) and (12) are balanced with respect to H and O [37,40]. Although the surface species indicated in reactions (11) and (13) divide out of the corresponding mass law expressions, they are included to emphasize the link between adsorption and surface precipitation. The term K_{PS}^{int} represents the intrinsic equilibrium constant for Al(III) precipitation, and K_{sp_Si} is the thermodynamic solubility product constant of $SiO_{2(s)}$. Importantly, only three of the four equations (10)–(13) are mathematically independent expressions. Table 2 presents the parameters used to model surface precipitation.
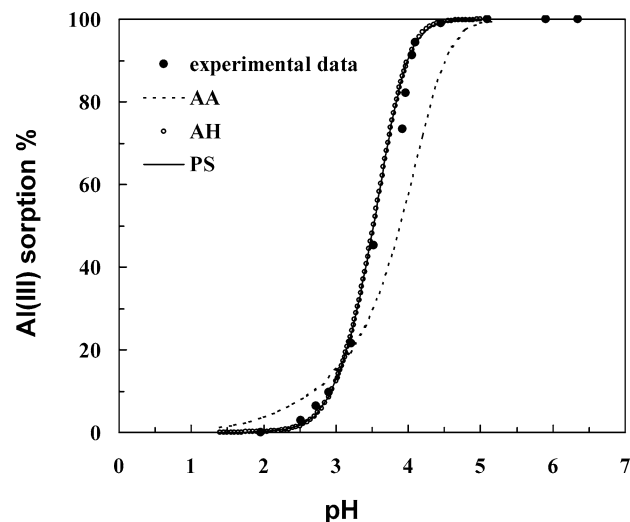

Fig. 1. Percentage of Al sorption vs pH and DLM simulation results of 1×10^{-4} M Al(III)/$SiO_{2(s)}$ system. Three predictions according to adsorption of Al^{3+} ion (AA), adsorption of $AlOH^{2+}$ ion (AH), and surface precipitation (PS) reactions are given for comparison. Fitting parameters are as follows: $\log K_{AA}^{int} = 0.5$, $\log K_{AH}^{int} = -3$, and $\log K_{PS}^{int} = -4.8$.

3. Results and discussion

3.1. Al(III) sorption and simulation of SCM/SPM

The effect of the change in the concentration of the background electrolyte (KNO_3) on the Al(III) sorption onto $SiO_{2(s)}$ was examined before the pH-edge and isotherm experiments to clarify the strength of the bonding between Al(III) and the $SiO_{2(s)}$ surface. The experimental results revealed that ionic strength did not affect the sorption of Al(III) onto $SiO_{2(s)}$ (figure not shown). This finding suggests that Al(III) tends to form an inner-sphere complex, which bonds strongly to the o-plane [41]. From previous studies, the structure of strongly sorbed surface species is generally described as monodentate or bidentate inner-sphere complexes at low and moderate surface coverage, and as multinuclear species and surface precipitation at high surface coverage [17–19,42].

Fig. 1 shows the model predictions of 1×10^{-4} M Al(III) reactions in $SiO_{2(s)}$ suspensions at various pH for the AA, AH, and PS configurations (Table 1) considered in SCM/SPM. The experimental results display that Al(III) sorption onto $SiO_{2(s)}$ increases with the pH value. The AH and PS configurations excellently fit the experimental data and both appear as one line, while the AA type does not satisfactorily describe Al(III) behavior in this region of the envelope curve. The results of the PB simulation were ignored because homogeneous Al hydroxides cannot precipitate in such a low initial concentration of Al(III), according to the solubility product constant of $Al(OH)_{3(s)}$. As the modeling results suggest, the adsorption mechanism dominates the uptake of 1×10^{-4} M Al(III). Crawford et al. [43] stated that the dielectric constant of the solid substrate plays a major role in determining the pattern of the complex species dur-
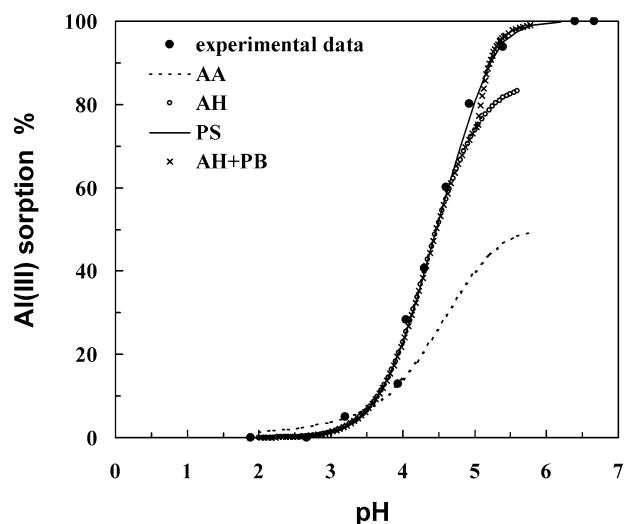
Fig. 2. Percentage of Al sorption vs pH and DLM simulation results of 1×10^{-3} M Al(III)/SiO$_{2(s)}$ system. Four predictions according to adsorption of Al^{3+} ion (AA), adsorption of AlOH^{2+} ion (AH), surface precipitation (PS), and adsorption of AlOH^{2+} ion incorporated with bulk precipitation (AH + PB) reactions are given for comparison. Fitting parameters are as follows: $\log K_{AA}^{int} = 0.5$, $\log K_{AH}^{int} = -4$, $\log K_{PS}^{int} = -5.8$.

Fig. 3. Modeling Al(III) sorption isotherm using diffusion-layer model. Four predictions according to adsorption of Al^{3+} ion (AA), adsorption of AlOH^{2+} ion (AH), surface precipitation (PS), and adsorption of AlOH^{2+} ion incorporated with bulk precipitation (AH + PB) reactions are given for comparison. Fitting parameters are as follows: $\log K_{AA}^{int} = 0.5$, $\log K_{AH}^{int} = -4$, $\log K_{PS}^{int} = -5.8$.

ing metal ion adsorption. The dominant sorbing species is the free metal ions when a solid substrate with a dielectric constant (ϵ) approaching that of water ($\epsilon = 78.3$) is used. However, the hydrolysis product of metal ions is the dominant adsorbing species when a solid substrate with a low dielectric constant is used. Accordingly, AlOH^{2+} is the dominant adsorbing species in this system since the dielectric constant of SiO$_2$ ($\epsilon = 6$) is much less than that of water.

Fig. 2 presents the model-predicted and experimental data for 1×10^{-3} M Al(III) reactions between SiO$_{2(s)}$ and solution as a function of pH. As illustrated, attempts to describe the pH-edge data using the adsorption of Al^{3+} ions (AA type in SCM) were unsuccessful above pH 3. This results could be attributed to the fact that the hydrolysis of free Al^{3+} ions occurs above pH 3, and the hydrolyzed species (AlOH^{2+}, Al$_2$(OH)$_2^{4+}$, and Al$_3$(OH)$_4^{5+}$) begin to dominate [44]. Simulation that involves the AH type successfully describes the interfacial behavior of Al(III) below pH 4, but significantly underestimates the experimental data above pH 4, where high surface loading occurs. Other combinations of reactions were considered to improve the fitness of predictions and explore the events that occurred at high pH. The predictions based on AH configuration incorporated with the reaction of homogeneous precipitation of Al(OH)$_{3(amporphos)}$ (in the database of the MINTEQA2 Program, v. 3.1) in bulk solution (PB) were denoted as crosses in Fig. 2. The AH + PB modeling curve has a discontinuous point at pH 5 and then rises gradually to meet the experimental data as pH increases. Consequently, the increase in the removal of Al(III) above pH 5 can be attributed primarily to Al hydroxide deposition in bulk solution. Two possible reasons account for the underestimation of SCM from pH 4 to 5: (a) saturation of SiO$_{2(s)}$ surface sites with increasing Al(III) sorption, and
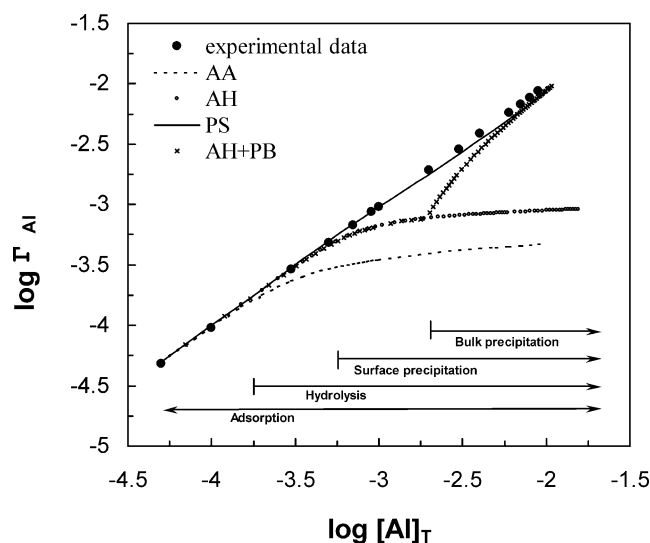
(b) failure to account for Al(III) polymerization and surface precipitation [31]. When the number of surface sites of SiO$_2$ is taken to be 8.35 μmol/m^2 (calculated by data in Table 2), the 1×10^{-3} M Al(III) sorbed by SiO$_2$ suspension in the range pH 4–5 occupies just 14% to 48% of the sites. This phenomenon implies that the postulate (a), insufficiency of surface sites for Al(III) removal, does not apply to this system because of the surface geometry [24]. With reference to postulate (b), Fig. 2 indicates that the surface precipitation model with the solid solution assumption reasonably fits the data over the whole range of experimental pH. Therefore, surface precipitation occurs at pH 4, which is about one pH unit lower than for homogeneous Al hydroxide precipitation. Over the pH range from 4 to 5, surface precipitation is the dominant reaction in this system. A number of researchers have demonstrated that the SCMs are satisfactory only for low surface loading, while SPM can provide reasonable fits to the data over a wide range of coverage conditions, from low to high [18,19,30,31,37,40,45]. Increasing the initial concentration of Al(III) by one order of magnitude (1×10^{-4}–1×10^{-3} M) results in a great variety of governing surface reactions; therefore, both the pH and the sorbate/sorbent ratio importantly affect sorbate reactions at the solid/solution interface.

The effect of sorbate-to-sorbent ratio on surface reaction is depicted using sorption isotherms at pH 4.80 ± 0.03 (Fig. 3), where total Al(III) concentration ($\log [Al]_T$) is plotted against sorption density ($\log \Gamma_{Al}$, where Γ_{Al} is mole Al(III) uptake per gram of SiO$_2$ solid). This isotherm experimental data plotted in double logarithmic format follow a linear trend with unit slope over the whole range of total Al(III) concentrations. Karthikeyan et al. [30,31] tested

the sorption of copper onto hydrous oxides of iron and aluminum and found out that the copper isotherms for both oxides have an initial region with unit slope at low total Cu and a Freundlich region with a slope of less than 1:1 at moderate Cu concentrations. A saturation region also exists, in which Cu removal increases sharply with total Cu, since all the sorbent reactive sites are fully occupied and Cu is removed by precipitation reactions. The linear and Freundlich regions in the isotherm can account for the two types of reactive sites high and low binding strength, for Cu uptake by iron or aluminum oxide surfaces. However, the isotherm data for Al(III) in this study all follow a linear trend with unit slope over the entire range of total Al(III) concentrations, even in the zone where homogeneous Al hydroxide precipitate may be formed. This result implies that there is only one reactive site with the same binding strength for Al(III) uptake by $SiO_{2(s)}$ surface, and at high Al(III) concentrations, some reactions lead to a transition between adsorption and bulk precipitation. Attempts to describe these isotherm data using SCM, illustrating adsorption of various Al species (AA and AH), SPM, assuming a solid solution formed on the surface (PS), and homogeneous precipitate of Al hydroxide in bulk solution (PB) are shown in Fig. 3. As illustrated in Fig. 3, all models yield suitable fits at low surface coverage, but only SPM reasonably fits the data at high surface coverage. Therefore, the onset and domains of adsorption, hydrolysis, surface precipitation, and bulk precipitation are delineated from the divergence between the model predictions and the isotherm data. Assuming adsorption of free Al^{3+} ions (AA) and $AlOH^{2+}$ (AH) resulted in the model's fitting satisfactorily up to a surface coverage of $10^{-3.25}$ mol Al(III)/g $SiO_{2(s)}$. This value of coverage also indicates the onset of surface precipitation. To clarify the surface and bulk precipitation, a homogeneous precipitation reaction of $Al(OH)_{3(s)}$ incorporated with the adsorption of $AlOH^{2+}$ (AH + PB) is also considered. In Fig. 3, the predictions using AH + PB include a discontinuous point at surface coverage of $10^{-2.75}$ mol Al(III)/g $SiO_{2(s)}$ and underestimate the range of surface coverage between $10^{-3.25}$ and $10^{-2.25}$ mol Al(III)/g $SiO_{2(s)}$, which can be regarded as the onset of the bulk precipitation of $Al(OH)_{3(s)}$ and the surface precipitation domain, respectively.

3.2. Evidences from electrophoretic mobility (EM) measurements

In the authors' earlier study, the EM of pure SiO_2 suspensions over a range of pH values and in three different salt solutions (0, 0.1, 0.5 M) lie on a curve and the isoelectric point (IEP) is 2.00 for an SiO_2 particle [34]. Therefore, 0.1 M KNO_3 was adopted as the background electrolyte in all experiments. Fig. 4 shows the EM data of SiO_2 suspension with various Al(III) concentrations as a function of pH. The electrophoretic behavior of SiO_2 with 1×10^{-5} and 1×10^{-4} M of Al(III) is similar to that of pure SiO_2 suspension. Meng and Letterman [13] also measured the
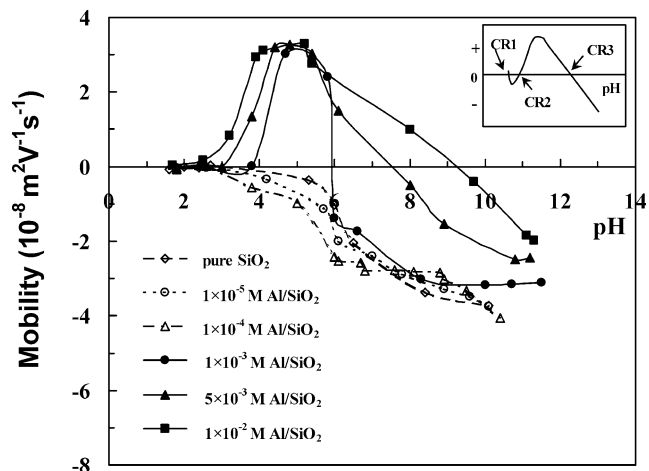

Fig. 4. The EM of Al(III)/SiO_2 suspensions as a function of pH in 0.1 M KNO_3 electrolyte in the presence or absence of various concentrations of Al(III).

zeta potential of Al(III)/$SiO_{2(s)}$ suspensions, but the tested Al(III) concentration was too high to observe electrokinetic behavior similar to that in pure SiO_2 suspension. James and Healy [20] examined the electrophoretic behavior of La(III) in a $SiO_{2(s)}$ suspension system and obtained similar results, with no significant shift in electrophoretic mobility, for low specific adsorption amounts of La(III).

Three charge reversal (CR) points (strictly, the pH values at which the electrokinetic potential reverses), CR1 (charge reversal from + to −), CR2 (charge reversal from − to +), and CR3 (charge reversal from + to −), correspond to increasing pH for the curves of SiO_2 with 1×10^{-3}, 5×10^{-3}, and 1×10^{-2} M of Al(III). The top right corner of Fig. 4 schematically depicts the general features of these electrokinetic curves, including charge reversals. Several recent spectroscopic studies [17,18,46,47] demonstrated that the value of 10% surface coverage is a criterion for the structure of surface complexes. The inner-sphere monomeric reactions can describe the sorption phenomenon in the low- and moderate coverage range (up to 10%). As coverage increases beyond 10% (high-coverage region), spectroscopic evidence is consistent with the formation of multinuclear species and surface precipitation. This study utilizes two coverage classification schemes, based on the percentage of occupied surface active sites and the area percentage covered by hydrated Al^{3+} ions with an assumed hydrated radius (H.R.) of 3 Å, to elucidate the surface electrophoretic behavior as a function of surface coverage. Table 4 presents the surface coverage values calculated at the 50% Al(III) uptake point on the pH edge for the specified conditions. Each pH edge yielded a range of surface coverages, extending from 0% to twice the value shown in Table 4. For the 1×10^{-5} and 1×10^{-4} M Al(III)/$SiO_{2(s)}$ systems with electrophoretic behavior similar to that of pure $SiO_{2(s)}$ suspension, both the coverage of the area and the site density are lower than 10%, within the range in which inner-sphere monomeric reactions occur [18]. Both the area and the site concentra-

Table 4
Surface coverage for Al(III) sorption pH edges in $SiO_{2(s)}$ suspension system

Total Al(III) conc. (mol/l)	Coverage of 50% uptake (μmol/m^2)	Coverage for area, H.R. of Al^{3+} = 3 Å (%)	Coverage for site concentration 1.67 mmol/g $SiO_{2(s)}$ (%)
1×10^{-5}	0.025	0.42	0.30
1×10^{-4}	0.25	4.24	2.99
1×10^{-3}	2.5	42.41	29.94
5×10^{-3}	12.5	212.06	149.70
1×10^{-2}	25	424.12	299.40

tion coverage of the 1×10^{-3}, 5×10^{-3}, and 1×10^{-2} M Al(III)/SiO$_{2(S)}$ system are beyond 10%, the electrophoretic behavior in these systems clearly differ from that of the 1×10^{-5} and 1×10^{-4} M Al(III)/SiO$_{2(s)}$ systems. Thus, the electrophoretic behavior reflects the mechanism of Al(III) sorption onto the surface of SiO$_{2(s)}$.

These experiments do not reveal any significant shift in CR1 with the concentration of Al(III). The significance of CR1 is clear in that H$^+$ and OH$^-$ ions are potential determinants for the original oxide; thus, CR1 is the point of zero charge (PZC) of the SiO$_2$ suspension.

Abundant evidence now supports the claim that at high pH charge reversal, CR3 reflects the metal hydroxide coating on the colloid substrate [20]. If sufficient metal ions are adsorbed at a pH suitable to form a complete coating of adsorbed metal hydroxide, then CR3 is the PZC of the metal hydroxide. Incomplete coating, due to a low concentration of metal or to a high concentration of colloidal substrate particles, reflects both coated and uncoated surfaces being mixed together. Thus, CR3 will occur at pH values at or below the pH$_{pzc}$ of the Al(OH)$_3$, depending on the coverage achieved. According to Fig. 4, CR3 is made to approach the pH$_{pzc}$ of amorphous Al(OH)$_3$ (9.0) [48] by increasing the Al(III) concentration. The CR3 of the colloid in the 1×10^{-2} M of Al(III)/SiO$_2$ suspension is the same as the pH$_{pzc}$ of pure Al(OH)$_3$, suggesting that Al(OH)$_3$ completely covered the SiO$_2$ particles.

In Fig. 4, the CR2 of the curves for SiO$_2$ with 1×10^{-3}, 5×10^{-3}, and 1×10^{-2} M of Al(III) ranges from pH 2 to 4 and increases as the concentration of Al(III) decreases. James and Healy [20] suggested that CR2 might indicate surface precipitation induced at a pH below that of bulk precipitation. They also used the relationship between standard free energy and the dielectric constants of the interfacial medium to derive the conclusion that the electric field of the surface-induced precipitation at the interface is established before bulk precipitation occurs, even though the solution is unsaturated with respect to this precipitated solid. Additionally, CR2 shifts to a lower pH as Al(III) concentration increases. Pugh and Bergström [49] also successfully interpreted the uptake of Mg(II) on α-ultrafine silicon carbide and α-alumina by applying James and Healy's model [20], and found that strong adsorption of Mg(II) occurred well below the bulk precipitation threshold. With respect to the 1×10^{-3} M Al(III)/SiO$_{2(s)}$ system, the CR2 in Fig. 4 is coincident with the point of the onset of surface precip-
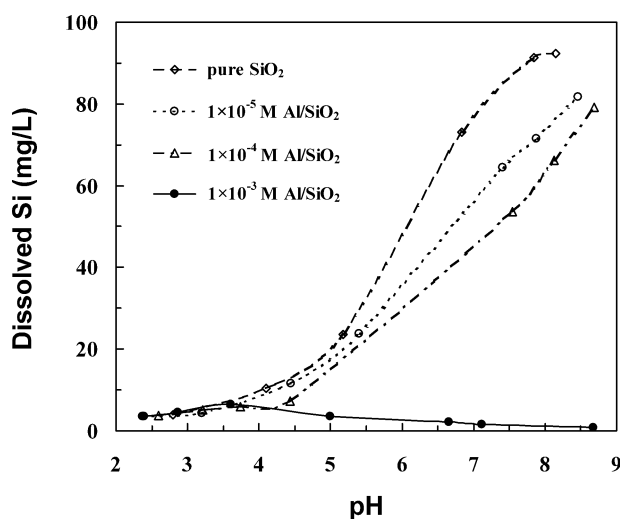

Fig. 5. Si dissolution of SiO$_{2(s)}$ suspension with or without Al(III) over a pH range 2–9.

itation (~pH 4) in Fig. 2, which was determined by the divergence between the SCM/SPM predictions and the experimental data. Accordingly, these electrokinetic findings confirm that the SPM, based on the solid solution assumption, can successfully describe the transition from adsorption to bulk precipitation and indicate the onset of surface precipitation. Furthermore, the occurrence of CR2 near the IEP of SiO$_{2(s)}$, almost obscuring it, could be regarded as representing the strong hydrolysis of Al(III) [20]. CR2 approaches CR1 in a strongly hydrolytic cation system but approaches CR3 in a weakly hydrolytic cation system.

3.3. Effect of Al(III) on SiO$_{2(s)}$ dissolution

Fig. 5 shows the solubility characteristics of 1 g SiO$_{2(s)}$/l suspension with or without Al(III) over the pH range from 2 to 9. The results imply that the release of silicate (represented as Si mg/l) from SiO$_{2(s)}$ solid increases with pH, perhaps because the ionization of monosilicic acid enhances the dissolution of H$_4$SiO$_4$ from SiO$_{2(s)}$, as illustrated below:

$$SiO_{2(s)} + 2H_2O \leftrightarrow Si(OH)_{4(aq)}, \tag{14}$$

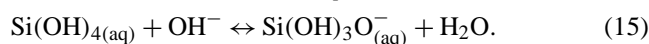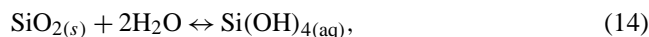$$Si(OH)_{4(aq)} + OH^- \leftrightarrow Si(OH)_3O^-_{(aq)} + H_2O. \tag{15}$$

Fig. 5 also indicates that the solubility of SiO$_{2(s)}$ decreases as the Al concentration increases. In a system with low Al(III) concentration, such as 1×10^{-4} and 1×10^{-5} M,

the concentration of the dissolved Si is slightly lower than that in a pure $SiO_{2(s)}$ system. Stumm and Wollast [50] reported that a surface-coordinated metal ion, such as Cu(II) or Al(III), can block an oxide surface group, thus suppressing dissolution. Aqueous Al(III) forms an aluminosilicate complex on the reactive silica surface site [1, Eq. (16)]; and this complex more strongly suppresses dissolution of the reactive silica surface in an alkaline medium than that in an acidic medium, as compared the dissolution in pure SiO_2 system.

$$-\overset{|}{\underset{|}{Si}}(OH) + Al(OH)_2^+ \leftrightarrow -\overset{|}{\underset{|}{Si}}\,OAl(OH) + H^+. \tag{16}$$
reactive silica surface site   aluminosilicate complex

In the system with a high Al concentration of 1×10^{-3} M, the concentration of dissolved Si is similar to that in the other systems below pH 4, but much lower than that in the pure $SiO_{2(s)}$ system above pH 4. The concentration of the Si in this system at pH 8.6 approaches 0.83 mg/l, which is two orders of magnitude less than that of the pure $SiO_{2(s)}$ system. Furthermore, the trend of the concentration of Si is quite different from that in other systems; the concentration increases with pH for pH < 4 but slightly drops as pH increases for pH > 4. These results imply that, while the surface aluminosilicate complex inhibits the dissolution of $SiO_{2(s)}$, other mechanisms may be responsible for the dramatic restraint of the dissolution. Stein [51] also observed the dissolution reduction of $3CaO \cdot Al_2O_3$ solid by surface precipitation of $Al(OH)_3$, but this reactivity reduction had been prevented by the presence of SiO_2. This different trend of dissolution in 1×10^{-3} M Al(III)/$SiO_{2(s)}$, can be explained by the formation of an Al hydroxide surface precipitate, which leads to a passive film on the surface of $SiO_{2(s)}$ and inhibits the corrosion of the $SiO_{2(s)}$ surface by OH^- ions.

4. Conclusions

Al(III) sorbs onto $SiO_{2(s)}$ in different modes at various pH and Al(III) concentrations, as an $Al(H_2O)_6^{3+}$ complex at low pH and Al(III) concentrations, hydrolyzed $Al(OH)(H_2O)_6^{2+}$ complex at medium surface loading, and surface-induced precipitate at high sorption densities, confirming earlier suggestions that sorption mode changes with surface loading [17–19,27]. The modeling results of the SCM/SPM prediction showed that the solution from which the surface precipitate formed was not saturated with respect to $Al(OH)_{3(s)}$. The SCM is an adequate model only when Al(III) sorption occurs as complexes binding at surface coordination sites of $SiO_{2(s)}$, while inconsistency between predicted behavior and data exists when solution conditions (alkaline pH, high sorbate/sorbent ratio) lead to the formation of surface precipitate. The SPM is capable of describing sorption over a wide range of pH and sorbate/sorbent ratios because this model allows species not only to sorb at the surface sites but also to form solid solutions on the

$SiO_{2(s)}$ surface. Electrokinetic measurements suggest that no significant shift in electrophoretic mobility occurs during the specific adsorption of Al(III) onto $SiO_{2(s)}$. However, under these solution conditions (1×10^{-3}, 5×10^{-3}, and 1×10^{-2} M Al(III)), which lead to surface precipitation, three charge-reversal points exist and separately represent the IEP of SiO_2, surface precipitation, and the Al hydroxide coating onto the SiO_2 surface. In the 1×10^{-3} M Al(III)/$SiO_{2(s)}$ system, CR2 (near pH 4) is coincident with the onset pH of surface precipitation, as determined by the SPM. The dramatically low concentration of dissolved Si above pH 4 in the 1×10^{-3} M Al(III)/$SiO_{2(s)}$ system is evidence of the formation of an Al hydroxide surface precipitate, which leads to the formation of a passive film on the surface of $SiO_{2(s)}$, inhibiting the corrosion of the $SiO_{2(s)}$ surface by OH^- ions.

Acknowledgments

References

[1] R.K. Iler, The Chemistry of Silica, Wiley, New York, 1979.
[2] C.T. Driscoll, K.M. Postek, in: G. Sposito (Ed.), The Environmental Chemistry of Aluminum, CRC Press, Boca Raton, FL, 1996, p. 363.
[3] D.W. Sparling, T.P. Lowe, P.G.C. Campbell, in: R.A. Yokel, M.S. Golub (Eds.), Research Issues in Aluminum Toxicity, Taylor & Francis, Washington, DC, 1997, p. 47.
[4] G.F.V. Landeghem, M.E.D. Broe, P.C. D'hases, Clin. Biochem. 31 (1998) 385.
[5] P. Nayak, Environ. Res. Sect. A 89 (2002) 101.
[6] S. Bi, S. An, W. Tang, R. Xue, L. Wen, F. Liu, J. Inorg. Biochem. 87 (2001) 97.
[7] T.W. Swaddle, Coord. Chem. Rev. 219–221 (2001) 665.
[8] B.A. Dempsey, H. Sheu, T.M.T. Ahmed, J. Mentik, J. Am. Water Works Assoc. 77 (1985) 74.
[9] R.D. Letterman, S.R. Asolekar, Water Res. 24 (1990) 931.
[10] G. Sposito, The Environmental Chemistry of Aluminum, second ed., Lewis Publishers, Boca Raton, FL, 1996.
[11] P.R. Anderson, M.M. Benjamin, Environ. Sci. Technol. 24 (1990) 692.
[12] P.R. Anderson, M.M. Benjamin, Environ. Sci. Technol. 24 (1990) 1586.
[13] X. Meng, R.D. Letterman, Environ. Sci. Technol. 27 (1993) 970.
[14] X. Meng, R.D. Letterman, Environ. Sci. Technol. 27 (1993) 1924.
[15] D.A. Kulik, Geochim. Cosmochim. Acta 64 (2000) 3161.
[16] J.D. Reid, B. NcDuffie, Water Air Soil Pollut. 15 (1981) 375.
[17] C.J. Chisholm-Brause, P.A. O'Day, G.E. Brown Jr., G.A. Parks, Nature 348 (1990) 528.
[18] L.E. Katz, K.F. Hayes, J. Colloid Interface Sci. 170 (1995) 477.
[19] L.E. Katz, K.F. Hayes, J. Colloid Interface Sci. 170 (1995) 491.
[20] R.O. James, T.W. Healy, J. Colloid Interface Sci. 40 (1972) 42.
[21] M. Rasmusson, S. Wall, Colloids Surf. A Physicochem. Eng. Aspects 122 (1997) 169.
[22] Y. Xu, F.W. Schwartz, S.J. Traina, Environ. Sci. Technol. 28 (1994) 1472.
[23] G.E. Millward, R.M. Moore, Water Res. 16 (1982) 981.

[24] W. Stumm, Chemistry of the Solid–Water Interface Processes at Mineral–Water and Particle–Water Interfaces in Natural Systems, Wiley–Interscience, New York, 1992.

[25] J.A. Davis, J.O. Leckie, J. Colloid Interface Sci. 67 (1978) 90.

[26] W. Stumm, E. Wieland, in: W. Stumm (Ed.), Aquatic Chemical Kinetics, Wiley–Interscience, New York, 1990, p. 367.

[27] N.T. Towle, J.R. Bargar, G.E. Brown Jr., G.A. Parks, J. Colloid Interface Sci. 187 (1997) 62.

[28] J. Laven, H.N. Stein, J. Colloid Interface Sci. 238 (2001) 8.

[29] K.G. Karthikeyan, H.A. Elliott, F.S. Cannon, Environ. Sci. Technol. 31 (1997) 2721.

[30] K.G. Karthikeyan, H.A. Elliott, J. Chorover, J. Colloid Interface Sci. 209 (1999) 72.

[31] K.G. Karthikeyan, H.A. Elliott, J. Chorover, J. Colloid Interface Sci. 220 (1999) 88.

[32] D.E. Yates, S. Levine, T.W. Healy, J. Chem. Soc. Faraday Trans. 70 (1974) 1807.

[33] L.S. Clesceri, A.E. Greenberg, A.D. Eaton, Standard Methods for the Examination of Water and Wastewater, APHA, AWWA, WEF, Washington, DC, 1998.

[34] W.H. Kuan, S.L. Lo, M.K. Wang, Water Sci. Technol. 42 (2000) 441.

[35] J.D. Allison, D.S. Brown, K.J. Novo-Gradac, MINTEQA2/ PRODEFA2, A Geochemical Assessment Model for Environmental Systems: Version 3.11 Database and Version 3.0 User's Manual, Environmental Research Laboratory, U.S. EPA, Athens, GA, 1991.

[36] D.A. Dzombak, F.M.M. Morel, Surface Complexation Modeling: Hydrous Ferric Oxide, Wiley, New York, 1990.

[37] K.J. Farley, D.A. Dzombak, F.M.M. Morel, J. Colloid Interface Sci. 106 (1985) 226.

[38] D.C. Thorstenson, L.N. Plummer, Am. J. Sci. 277 (1977) 1203.

[39] P.D. Glynn, E.J. Reardon, Am. J. Sci. 290 (1990) 164.

[40] J.A. Meima, R.N.J. Comans, Environ. Sci. Technol. 32 (1998) 688.

[41] K.F. Hayes, C. Papelis, J.O. Leckie, J. Colloid Interface Sci. 125 (1988) 717.

[42] M. Berka, I. Bányai, J. Colloid Interface Sci. 233 (2001) 131.

[43] R.J. Crawford, I.H. Harding, D.E. Mainwaring, Langmuir 9 (1993) 3057.

[44] C.F. Baes, R.E. Mesmer, The Hydrolysis of Cations, Wiley, New York, 1976.

[45] D.A. Dzombak, F.M.M. Morel, J. Colloid Interface Sci. 112 (1986) 588.

[46] C.J. Chisholm-Brause, K.F. Hayes, A.L. Roe, G.E. Brown Jr., G.A. Parks, J.O. Leckie, Geochim. Cosmochim. Acta 54 (1990) 1987.

[47] A.L. Roe, K.F. Hayes, C.J. Chisholm-Brause, G.E. Brown, G.A. Parks, J.O. Leckie, Langmuir 7 (1991) 367.

[48] G.A. Parks, Chem. Rev. 65 (1965) 177.

[49] R.J. Pugh, L. Bergström, J. Colloid Interface Sci. 124 (1988) 570.

[50] W. Stumm, R. Wollast, Rev. Geophys. 28 (1990) 53.

[51] H.N. Stein, in: G.H. Stewart (Ed.), Science of Ceramics, Academic Press, London, 1967, p. 109.